Characterisation of Stress Corrosion Cracking and Internal Oxidation of Alloy 600 in High Temperature Hydrogenated Steam

Characterisation of Stress Corrosion Cracking and Internal Oxidation of Alloy 600 in High Temperature Hydrogenated Steam

J. Lindsay[1], F. Scenini[1], X. Zhou[1], G. Bertali[1], R.A. Cottis[1], M.G. Burke[1], F. Carrette[2], F. Vaillant[2]

[1] Materials Performance Centre, The University of Manchester, Sackville Street Campus; Manchester M13 9PL, UK

[2] EDF (Electricite De France) R&D, MMC, Site des Renardieres; Moret sur Loing cedex 77818, France

Abstract

In this study, the possibility of using low pressure hydrogenated steam, which is capable of reproducing similar oxidising electrochemical potentials, has been examined. The oxides formed between 350°C and 500°C in low pressure steam have been characterised and compared to oxide that formed in high pressure water in autoclave tests at 350°C. The comparison shows that the oxides formed are similar but not identical. However, constant load tests carried in hydrogenated steam at 400°C showed a similar trend to the classical dependency of PWSCC as a function of potential. The oxides formed in both environments were characterized via FIB and AEM techniques. At 500°C internal oxidation and preferential oxidation of grain boundaries was observed but only on samples that were prepared by OPS. Conversely, those samples ground to 600 grit revealed a continuous and protective oxide. At lower temperatures the internal oxidation was almost suppressed, although the effect of surface preparation was still present and had a clear influence on the SCC test carried out at 400°C. Cr-rich carbides in the alloy appeared to accelerate the oxidation in the both the bulk and along the grain boundaries. This was observed for both steam and autoclave-exposed specimens.

AEM characterisation of the exposed specimens has been employed to determine the preferential oxidation rates and associated Cr depletion. The observed intergranular Cr-depletion was asymmetric and it was estimated that a two orders of magnitude difference in diffusivity were required to account for the observed difference.

Keywords: Hydrogenated Steam, Alloy 600, Internal Oxidation, Preferential Oxidation, Microstructure, FIB, AEM, Surface Finish

Introduction

It has long been known that Alloy 600 is susceptible to primary water stress corrosion cracking (PWSCC), which is a form of intergranular stress corrosion cracking (SCC). The mechanism responsible for PWSCC in Alloy 600 is still under debate, although there is growing evidence in support for Scott and Calvar's [1] model of internal oxidation (IO), in which grain boundary oxidation is responsible for embrittlement and cracking.

The IO model was based on the high temperature phenomena that occurs in a number of alloys in which the mechanical properties were compromised as a result of an oxidant diffusing into the matrix and reacting with the less noble alloying elements to form discrete oxides [2, 3]. The depth of the internally-oxidised zone (ξ) can be calculated by Wagner's equation (equation 1). This assumes that the internal oxidation is diffusion-controlled and only oxide precipitates form, with no scale oxide formed on the surface.

$$\xi = \left(\frac{2N_O^S D_O t}{\nu N_B^0}\right)^{1/2} \qquad \text{Equation 1}$$

where N_O^S is the solubility of the oxidant, D_O is the diffusivity of the oxidant, t is the exposure time, N_B^0 is the concentration of the reactive element in the alloy and ν is the stoichiometric value of the oxidant when reacting to form the oxide particles [2, 4]. It is from this equation that a large proportion of the oxygen diffusivity data in Ni is derived. Initial concerns on the IO model were raised as the solid state diffusion of oxygen in the alloy was not sufficient to sustain the cracking, based on the extrapolation of the high temperature data [5]. However, a number of authors have shown that there is significant preferential oxidation of grain boundaries at the temperature at which PWSCC occurs, and it has been suggested that the availability of Cr to form the oxide may be the rate-limiting step [6-9] .

Oxidation and PWSCC testing on Alloy 600 is typically performed in high temperature, pressurised autoclaves. However, some work has been done in low pressure hydrogenated steam. Economy and Jacko [10, 11] demonstrated that there is a continuum in the SCC mechanism up to 400°C in high pressure (200 bar) steam whilst Capell and Was [12, 13] have used low pressure steam to simulate SCC.

Results from both steam and water tests have shown that the surface finish affects the oxide morphology. Autoclave testing has also shown different oxide penetration with different finishes as a result of a deformed surface layer [7, 14].

This study examines the oxides (internal and external) formed during autoclave tests and equivalent low pressure hydrogenated steam. SCC tests were performed at 400°C in hydrogenated steam over a wide range of oxygen partial pressures related to the occurrence of PWSCC. The purpose of this investigation was to investigate whether it was possible to reproduce the same morphology of PWSCC in the steam environment. The effect of surface finish on both the oxidation and SCC was also examined.

Experimental Procedures

WF675, a forged heat of Alloy 600 which has been used for control rod drive mechanism (CRDM) nozzles, was used for oxidation and SCC studies. This heat is known to be highly susceptible to PWSCC [15]. The chemical composition of the alloy is shown in Table 1. Oxidation studies were conducted on corrosion coupons (20×19×2 mm^3) obtained from WF675 in two conditions: 1) the as-received (AR) material which was in the as-forged condition and 2) cold-worked (CW) in tension to a strain of 15%. PWSCC tests and characterisation have been performed on these materials by various

authors [7, 15, 16]. In the present study the surfaces of the samples were finished with either a P600 SiC paper or a 60 nm oxide polishing suspension (OPS). The P600-finished samples had a deformed layer in the order of 2 µm, was detected via FIB cross-sectioning, consistent with the values reported in the literature for stainless steel with a comparable finish [17]. The OPS-polished samples were considered to be a strain-free surface on the basis that it is commonly used to prepare samples for EBSD analysis when the Bielby layer must be removed.

Dog-bone samples were used for the SCC tests. These samples were extracted from WF675 which was cold-rolled to 19%. The specimen orientation was such that the applied load in the SCC tests was in the transverse direction of cold-rolling and crack propagation would occur in the longitudinal direction. This orientation was chosen as it has been shown to be one of the most susceptible to PWSCC [15, 18]. In order to investigate the effect of surface preparation, the tensile samples had one side polished to an OPS finish and the opposite surface ground with P600 paper.

Oxidation tests were conducted in a hydrogenated steam environment; with the temperature range of 350°C to 500°C for 500 h with R equal to 20. In order to have a direct comparison to steam test data, an autoclave test was also performed in high purity (no lithium or boron), hydrogenated (30 cc/kg of dissolved hydrogen) water at 350°C for 500 h.

The hydrogenated steam oxidation system used has been described by Scenini et al. [19]. For convenience, a parameter *R* has been used to describe the oxidising potential of the hydrogenated steam environment. This parameter *R*, used in preference to the electrochemical potential (which is meaningless in a non-conductive medium) is the ratio between the partial pressure of O_2 at the Ni/NiO transition point and the partial pressure of O_2 in the system used. It is well-known that the maximum susceptibility of PWSCC occurs around the Ni/NiO transition [10, 20] which in this case would correspond to R=1. For instance if R=8, it implies that there is eight times less oxygen than required to oxidise Ni. The full derivation of the thermodynamic calculations can be found in [19].

$$\mathrm{R} = \frac{\mathrm{PO_2}_{\mathrm{Ni/NiO}}}{\mathrm{PO_2}} \qquad \text{Equation 2}$$

The dissociation partial pressure at the Ni/NiO transition was confirmed at 400°C with the use of Ni 200 (99% pure Ni) coupons exposed in a different gas constituent. For R values less than one (0.3 and 0.7), both visual inspection and grazing angle X-ray diffraction confirmed the presence of an oxide whilst no oxide was found at R values greater than 1 (R=7). It is however important to point out that this system has its limitation in terms of accurately controlling the environment to R=1 and therefore most of the tests were performed astride this value.

The SCC tests were conducted under constant load in a hydrogenated steam environment similar to the system described above and in ref [19]. However, for these tests the reaction chamber was vertically mounted within a 10 kN Instron tensile machine. In addition, the reaction tube was single-walled Ni 200 with an inner coil used to preheat the flowing steam.

Microstructural Characterisation

Light optical microscopy (LOM) was used to evaluate the microstructure of the as-received and cold-worked forging material prior to SCC and oxidation tests. Other analytical techniques employed in this investigation included x-ray diffraction (XRD), scanning electron microscopy, focused ion beam

(FIB) microscopy and FIB specimen preparation, and analytical electron microscopy. An FEI Quanta 650 field emission gun (FEG) scanning electron microscope (SEM) equipped with an Oxford Instruments X-max 50 Silicon Drift Detector and AZTEC analyser and electron backscattered diffraction (EBSD) system, and a Zeiss Ultra 55 FEG SEM equipped with an Oxford Instruments EDX analysis system were used to characterise the oxidised and stress-corroded specimens. An FEI Quanta 3D FIB was used to prepare site-specific specimens for TEM characterisation and to examine various regions of the specimen in cross-section (FIB-SEM).

Detailed characterisation of the microstructure and near-surface regions after exposure in hydrogenated steam was performed using an FEI Tecnai F30 300 kV FEG analytical electron microscope (AEM) equipped with an Oxford Instruments X-max 80 SDD and INCA/AZTEC analysis system.

Results

TEM analysis of the AR forging indicated that it consists of a mixed recrystallized and recovered/ hot worked microstructure (Figure 1a, b). The microstructure was also characterised by the presence of a high proportion of both intragranular and intergranular Cr-rich M_7C_3 carbides, and a few very fine (<50 nm in size) intergranular $M_{23}C_6$ carbides along portions of some grain boundaries. The ¬19% cold-rolled material exhibited a very high proportion of fine slip bands and dislocations. This highly-deformed structure appeared to overwhelm the subgrain structure to produce a relatively homogenous microstructure, Figure 1c.

Several tensile tests were performed using steam oxidation rig to characterize the materials at 400°C. The yield stress of the cold-worked material was 610 MPa and the UTS was 690 MPa; however, these values do not account the seal/pull rod friction. The SCC tests were conducted just above the yield point at 630 MPa. Tests were conducted over a range of R values, for each test specimen the largest crack was measured, these results are shown in Figure 2.

All samples that failed by SCC had the initiation sites on the OPS surface only (Figure 3). Figure 4 shows that significantly more cracks were formed on the OPS surface relative to the P600. Quantitative analysis of SEM images of both specimen surfaces at equivalent locations were analysed in terms of the number of detected cracks and their length (Figure 5).

The oxides formed on both the OPS and P600 surfaces during exposure in the high-pressure water autoclave tests were evaluated using FEG-SEM (Figure 6) and cross-sectioned using the FIB technique (Figure 7). The oxide on the OPS surface, which is likely to be Cr oxide [9], appears to have a defined crystallographic orientation with respect to the matrixes; the thickness of the oxide varies significantly between grains. The oxide on the P600 is expected to be Cr oxide with Ni-Fe-Cr spinel, as reported in the literature [9]. The globular structure of the internal oxides (the assumption that it was a oxide is based on the similar results seen by [7] and the fact that the contrast of the feature was consistent and connected to the surface oxide) observed in the WF675 may be a result of the microstructure of the alloy.

FIB cross-sections of the steam oxidised samples showed that internal oxidation of the matrix had occurred on the tests carried out at 500°C on the OPS surface (Figure 8 and Figure 9), the P600 grit however only formed an external Cr oxide (Figure 8). Using Wagner's equation the diffusivity of

oxygen in the bulk can be calculated. The given internal oxidation depths are the maxima, this is justified as grains with less internal oxidation (extreme cases none) had more significant surface oxidation and as such do not meet the conditions under which Wagner's equation was derived. In addition to the internal oxidation, preferential oxidation of the grain boundaries and slip bands was observed. The maximum observed depth of intergranular and internal oxidation are shown in Table 2. There was a significant variation in the extents of both internal and preferential intergranular oxidation in the AR material, in contrast to the more uniform oxidation in the cold worked material. However, these observations were based on limited data sets.

For both steam and autoclave testing, it was observed that the Cr-rich carbides were oxidised. There is some evidence, although based on limited examples, that the depth of oxide penetration may be increased by their presence (Figure 9).

TEM specimens were obtained from preferentially-oxidised grain boundaries in the 500°C 66 h test using FIB. Semi-quantitative STEM-EDX microanalysis data revealed the presence of Cr-depleted regions that were associated with the formation of the intergranular oxides. All but one of the observed Cr-depleted regions observed displayed an asymmetry, with one grain having a significantly larger depleted zone than the other (Figure 10). The extreme case of the asymmetry was a depleted zone of 750 nm compared to 50 nm in the other grain. In addition to there being significant depletion in the grains adjacent to the formed oxide, the grain boundary in advance of the oxide was found to be significantly depleted in the same asymmetrical manner. The full extent of this depletion could not be characterised as the presence of small $M_{23}C_6$) carbides on the grain boundaries skewed the data, however in some observed samples the depleted zone in advance of the oxide exceeded 4 μm (beyond the end of the TEM sample), in other cases it was limited to 200 nm. The Cr-depleted grain boundaries were Ni-enriched and Fe-depleted. Furthermore Ti, Al and O enrichments were present in the Cr-rich oxide and several tens of nanometres ahead of it.

Discussion

The data generated in this study have shown that SCC in the hydrogenated steam environment is consistent with PWSCC with respect to the fracture morphology (Figure 3) and potential dependency (Figure 2), which was similar to that reported in high pressure autoclave tests at lower temperatures. This supports to the use of low pressure steam as an alternative test method.

The use of low pressure steam at the same temperatures as the high pressure autoclave tests show that the preferential oxidation rates are significantly less in equivalent tests as can be seen in Table 2Table **1**. This well know effect [21] has been attributed to the pressure differences in the environments and not indicative of a different environment, this is based on the consistencies in the structure of preferential oxides formed with only magnitude varying.

The oxidised as-received material exhibited an internal oxide which was in the form of interconnected particles, which form on the grain boundaries, some grains exhibiting an oxide of uniform thickness which follows the grain boundary directly. The cold-worked samples exhibited a continuous oxide of uniform thickness on all the observed oxidised grain (Figure 1). It is postulated that the observed difference in preferential oxidation is a result of the difference in microstructure,

specifically the presence of a strong subgrain structure in the as-forged material (Figure 1) which produces local differences in the oxidation rate as it proceeds along a boundary, thus resulting in variable thicknesses in the grain boundary oxide, whist the cold worked material produces a oxide of uniform thickness.

It should be noted that the grain boundary oxides on both materials were continuous (both in steam and water) and connected, as such they should be referred to as a preferential oxidation, not the internal oxidation implied by the suggested mechanisms name.

The stress-free surface obtained by OPS polishing was significantly more susceptible to SCC and agrees with results by Scenini et al. at 400°C in high pressure steam [14]. Although the deformed layer with a rough surface would be expected to be detrimental to SCC initiation, the deformed layer will increase the diffusivity of both O and Cr in the alloy, but the increased outward diffusivity of Cr promotes the external oxide formation which inhibiting the inward diffusion of O [19, 22]. This transition between external and internal intergranular oxide as a result of surface finish was observed in both the steam and autoclave testing (Figure 7 and Figure 8).

The oxide formed in autoclave testing is reported in the literature to be a Cr oxide film with Ni-Fe-Cr spinel oxides formed on top [9], this is the same as the oxide formed in the present work on the P600 surface. However, the use of a stress-free surface in the same test produced a crystallographic oxide with no spinels (Figure 6). The rotation in the oxide at a twin in this image illustrates the crystallographic nature of the oxide). The formation of the Ni nodules in the 500°C steam may be seen as the result of the outward diffusion of Ni, as a result of Ni rejection and stress build up associated with the formation of an internal/preferential oxidation [23]. This mechanism is supported by the fact that no Ni rejection was detected on samples that do not undergo internal oxidation such as P600 surfaces.

The preferential oxidation of carbides in both steam and autoclave testing was observed. These results (e.g. Figure 9) are in contrast with the formulated hypothesis Cr carbides are beneficial to PWSCC because they act as oxygen traps [24]. However, the carbides appear to be responsible for an increase the oxidation rate on both the grain boundaries and in the internal oxides. Furthermore, in the case of the internal oxides, the oxide formed changes from discontinuous to continuous in the presence of the carbides. This observation may be attributed to the incoherent boundary at the carbide/matrix interface resulting in enhanced oxygen diffusivity and/or the carbide acting as a Cr source. The latter case would support the suggestion that the limiting condition in the oxidation is the availability of Cr, not oxygen [25].

The presence of a titanium and aluminium oxide in advance of the Cr oxide is significant but not unexpected and the might have a role in the intergranular oxide penetration [23].

Examples of an asymmetric Cr depletion were observed for numerous examples of preferential intergranular oxidation. Based on this asymmetry and simple calculations from $x^2 = 2Dt$, with x equal to the depleted zone width, t is the time at temperature, and D is the diffusivity, the observed asymmetry in the depleted width required a difference in the Cr diffusivity of two orders of magnitude on the adjacent grains.

Based on Wagner's equation (equation 1), the bulk diffusivity of oxygen in the alloy was calculated, and the results were consistent with the literature.

Based on the data in Table 2 and calculating the values of K_{oxide} it is seen that the values are significantly less than what was calculated by Scott et al [1], (Figure 11). However, it should be noted that initial results from an on-going study has shown that there appears to be an effect of residual stress on the oxidation rate [23]. Also, there is a three orders of magnitude difference in K_{oxide} between the steam and high pressure water tests at 350°C.

Although cold-worked specimens were more susceptible than the as-received WF675 specimens to PWSCC, the maximum observed oxide penetration depths were consistent (Table 2) between the samples. However, it was noted that the as-received samples showed considerable variability in depth of oxidation in contrast to the relatively uniform depth of oxidation observed in the cold-worked samples. It is speculated that the mixed microstructure present in the as received forged structure is responsible for the variation.

Conclusions

The results of this investigation can be summarised in the following bullet points:

- SCC in hydrogenated steam exhibited a similar potential dependency to that observed in lower temperature autoclave PWSCC tests with the fracture surfaces observed been consistent with the path and morphology of the preferential oxides formed on the grain boundaries.

- The mechanically-prepared surfaces were less susceptible to SCC compared to a polished surface with no deformed layer.

- Internal oxidation, both classical and preferential grain boundary oxidation was observed in specimens exposed in 500°C steam. Conversely, only preferential intergranular oxidation was detected in specimens tested in the autoclave at 350°C and in steam at 350°C and 400°C.

- The preferential intergranular oxidation observed in the steam-exposed specimens occurred at a low rate compared to that in specimens exposed in pressurised autoclaves.

- Preferential oxidation rates were measured and compared to the diffusivity of oxygen that Scott predicted for his PWSCC. The measured values were not consistent with Scott's prediction, but the results from high pressure autoclave tests were closer than results obtained at atmospheric pressure, all tests were carried out with no applied load which may provide an explanation for the discrepancy.

- Carbides appeared to accelerate both internal and preferential intergranular oxidation and this finding was discussed in terms of Cr availability and diffusivity.

- Asymmetric Cr-depletion associated with the intergranular oxide was detected in specimens tested in hydrogenated steam.

References

1. Scott, P.M. and M. Le Calvar. *Some Possible Mechanisms of Intergranular Stress Corrosion Cracking of Alloy 600 in PWR Primary Water*. in *Sixth International Symposium on Environmental Degradation of Materials in Nuclear Power Systems--Water Reactors; San Diego, California; United States; 1-5 Aug. 1993. pp. 657-667.1993*. 1993: The Minerals, Metals & Materials Society.
2. Douglass, D.L., Oxid. Met, 1995. **44**(81).
3. Wood, G.C., et al., *The High Temperature Internal Oxidation and Intergranular Oxidation of Nickel--Chromium Alloys.* Corrosion Science, 1983. **23**(1): p. 9-25.
4. Gleeson, B., ed. *Shreir's Corrosion*. 1.09 Thermodynamics and Theory of External and Internal Oxidation of Alloys, ed. T.J.A. Richardson. 2010, Oxford.
5. Staehle, R.W. and Z. Fang. *Comments on a proposed mechanism of internal oxidation for Alloy 600 as applied to low potential SCC*. in *9th Environmental Degradation of Materials in Nuclear Power Systems--Water Reactors; Newport Beach, CA; USA; 1-5 Aug.* . 1999: Minerals, Metals and Materials Society/AIME.
6. Scott, P.M. and P. Combrade, *On the mechanism of stress corrosion crack initiation and growth in alloy 600 exposed to PWR primary water*, in *In Eleventh international conference on environmental degradation of materials in nuclear power systems – water reactors*. 2003.
7. L. Fournier, et al., *Grain Boundary Oxidation and Embrittlement Prior to Crack Initiation in Alloy 600 in PWR Primary Water*, in *15th International Conference on Environmental Degradation of Materials in Nuclear Power System – Water Reactors*. 2011: Colorado Springs.
8. Matthew J. Olszta, et al., *Electron Microscopy Characterizations and Atom Probe Tomography of Intergranular Attack in Alloy 600 Exposed to PWR Primary Water*, in *15th International Conference on Environmental Degradation of Materials in Nuclear Power System – Water Reactors*. 2011.
9. Combrade, P., et al. *Oxidation of Ni base Alloys in PWR Water: Oxide Layers and Associated Damage to the base Metal* in *Twelfh International Symposium on Environmental Degradation of Materials in Nuclear Power Systems-Water Reactors, Salt Lake City, UT, USA, 14-18 August* 2005: Minerals, Metals and Materials Society/AIME.
10. Economy, G., R.J. Jacko, and J.A. Begley. *Influence of Hydrogen Partial Pressure on the IGSCC Behavior of Alloy 600 Tubing in 360 C Water or 400 C Steam*. in *Corrosion, 87/92*. 1987: NACE International.
11. Economy, G. and R.J. Jacko, *IGSCC Behavior of Alloy 600 Steam Generator Tubing in Water or Steam Tests Above 360 deg C.* Corrosion, 1987. **43**(12): p. 727- 734.
12. Brent Capell, L.F., and Gary S. Was, University of Michigan, *Intergranular Cracking Behavior of Ni-xCr-9Fe-C Alloys in Hydrogenated Stream.* Tenth International Symposium on Environmental Degradation of Materials in Nuclear Power Systems--Water Reactors; Lake Tahoe, Nevada; USA; 5-9 Aug. 2001, 2001.
13. Capell;, B.M. and G.S. Was, *Selective Internal Oxidation as a Mechanism for Intergranular Stress Corrosion Cracking of Ni-Cr-Fe Alloys* Metall. Trans., 2007. **38**(6): p. 1244-1259.
14. Scenini, F., et al., *Effect of Surface Preparation on Intergranular Stress Corrosion Cracking of Alloy 600 in Hydrogenated Steam.* Corrosion, 2008. **64**(11): p. 824-835.
15. Léonard, F., *Study of Stress Corrosion Cracking of Alloy 600 in High Temperature High Pressure water.* 2010, University of Manchester.
16. F. Leonard, et al., *The Role of Lattice Curvature on the SCC Susceptibility of Alloy 600* in *15th International Conference on Environmental Degradation of Materials in Nuclear Power System – Water Reactors.* 2011: Colorado Springs.

17. Tegart, W.J.M., *The electrolytic and chemical polishing of metals in research and industry*. 1959: London : Pergamon, 1959.
18. Moshier, W.C. and C.M. Brown, *Effect of cold work and processing orientation on stress corrosion cracking behavior of {A}lloy 600.* Corrosion, 2000. **56**: p. 307--320.
19. Scenini, F., et al. *Oxidation Studies Related to PWSCC*. in *Twelfh International Symposium on Environmental Degradation of Materials in Nuclear Power Systems-Water Reactors, Salt Lake City, UT, USA, 14-18 August* 2005: Minerals, Metals and Materials Society/AIME.
20. Morton, D.S., et al. *Nickel Alloy Stress Corrosion Cracking in Deaerated Water: The Role of Environment*. in *EPRI Mitigation Working Group Meeting; May 18*. 2005.
21. A Fry, S Osgerby, and M. Wright, *Oxidation Of Alloys In Steam Environments - A Review*, in *Principles of Steam Oxidation*. 2002, NPL Report MATC(A)90, September 2002.
22. Scenini, F., et al. *Influence of PWSCC behaviour of Alloy 600 on its oxidation behaviour*. in *Corrosion 2007, Paper #07611*. 2007: NACE International.
23. Giacomo Bertali, et al., *OXIDATION STUDIES OF ALLOY 600 IN LOW PRESSURE HYDROGENATED STEAM*, in *16th International Conference on Environmental Degradation of Materials in Nuclear Power System – Water* 2013.
24. Panter, J., et al., *Influence of oxide films on primary water stress corrosion cracking initiation of alloy 600.* Journal of Nuclear Materials, 2006(348): p. 213–221.
25. Guerre, C., et al., *STRESS CORROSION CRACKING OF ALLOY 600 IN PWR PRIMARY WATER : INFLUENCE OF CHROMIUM, HYDROGEN AND OXYGEN DIFFUSION*, in *15th International Conference on Environmental Degradation of Materials in Nuclear Power System – Water Reactors. 2011*. 2011: Colorado Springs.

Table 1: Chemical composition of WF675.(wt.%)

	Ni	Cr	Fe	C	Mn	Si	S	P	Cu	Co	Al	Ti
WF 675	73.2	16.05	8.8	0.058	0.81	0.45	< 0.001	0.007	0.02	0.04	0.29 (Al + Ti)	

Table 2. Summary of the maximum depth of internal and preferential oxidation observed from the FIB cross-sectioned samples. All depths are the maxima and are measured normal to the surface, independent of the observed oxidation path.

Temperature (°C)	Duration (h)	Maximum observed depth of grain boundary oxidation (nm)		Maximum observed depth of internal oxidation (nm)	
		AR	CW	AR	CW
500	66	1390	1460	270	260
500	500	3100	2500	2070	1700
400	500	-	285	-	-
350 (Steam)	500	50	105	-	-
350 (autoclave)	500	670	1060	-	-

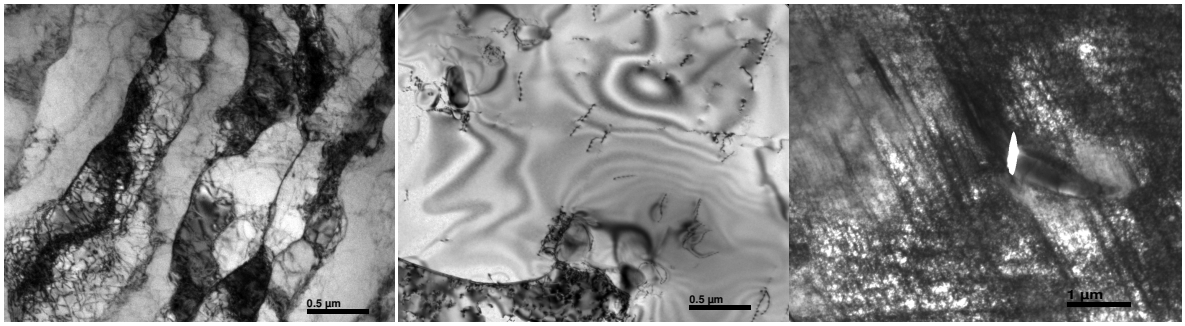

a b c

Figure 1. TEM images of the AR (as-forged) microstructure of WF 675 (a and b) showing the subgrain structure present in the recrystallized grains (a) and a recovered grain (b). The heavily deformed structure present in the cold rolled material, images includes a cracked carbide.

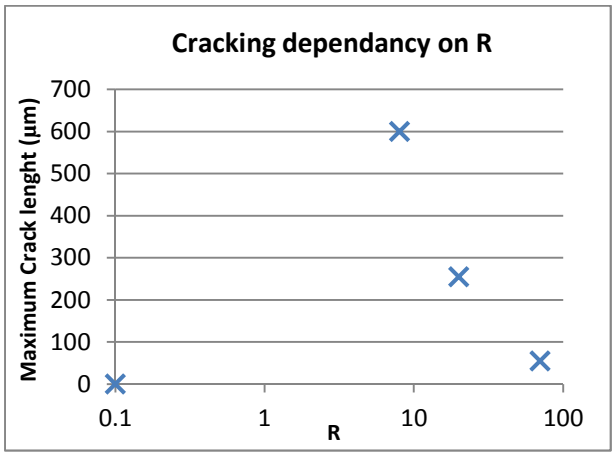

Figure 2. The cracking suceptiblity in 400°C hydrogenated steam as a function of the ratio (R). The data show a peak when the partial pressure of oxygen in the sytem is in the region of the partial pressure of Ni/NiO transition point.

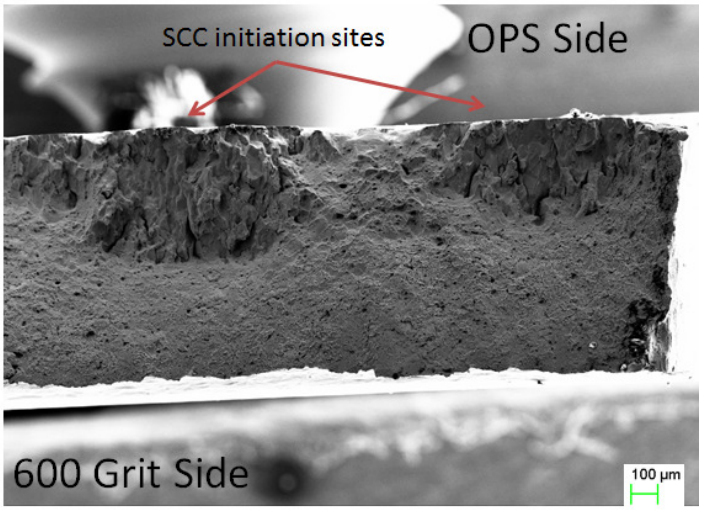

Figure 3. Secondaray electron (SE) image showing the fracture morthologdy of a cold-worked sample in the hydrogenated steam. No iniation was observed from the P600 surface.

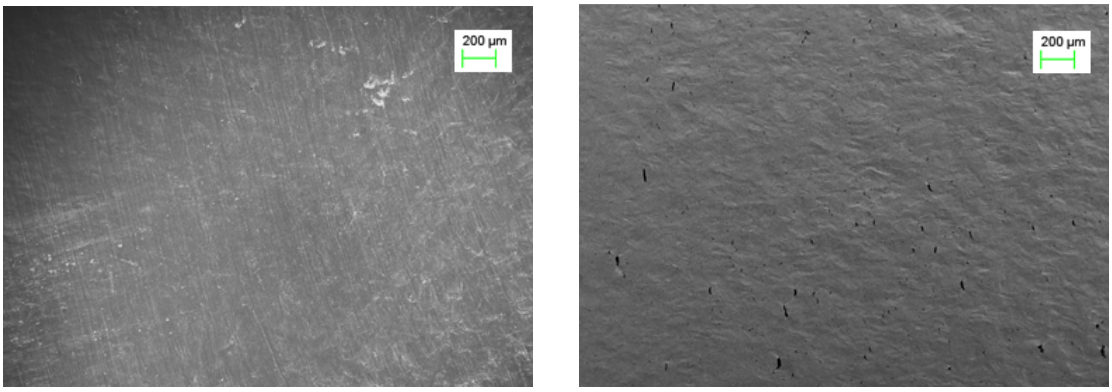

a b

Figure 4. SE images of the specimen surfaces from a test sample which failed by SCC. (a) P600-ground surface, and (b) OPS-polished surface. The load was applied in the horizontal direction, relative to the presented images.

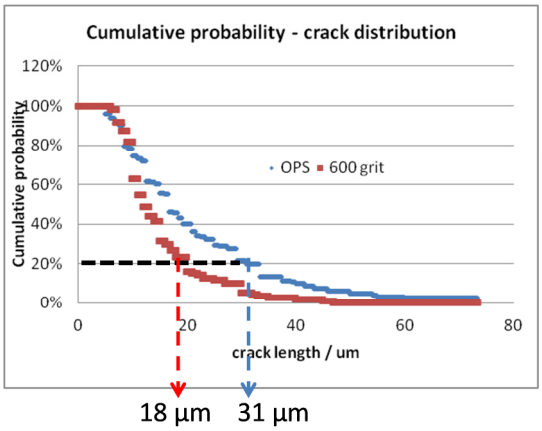

Figure 5. Cumulative crack probability distribution, the data is from a sample found to fail by SCC and consist of 149 cracks on the OPS surface whist only 96 on the P600, taken from the same size area on equivalent areas of the same sample.

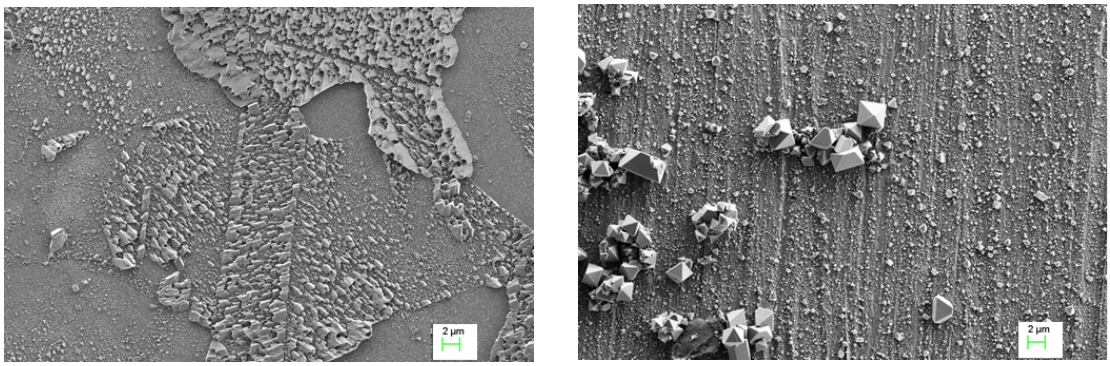

a b

Figure 6. SE images of surface morphology of the oxide formed on the OPS (a) and P600 (b) surfaces after 500 h of exposure to simulated PWR conditions.

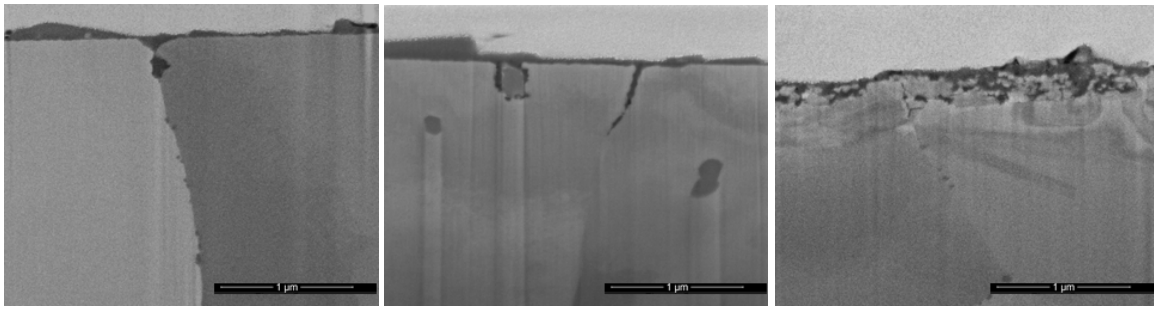

a b c

Figure 7. (a)-(b) FIB SE images showing the preferential darkly-imaging features formed on the OPS surface for the AR and CW samples respectively. (c) iFIB SE image of the cross-section of the P600 surface that had no preferential grain boundary oxidation.

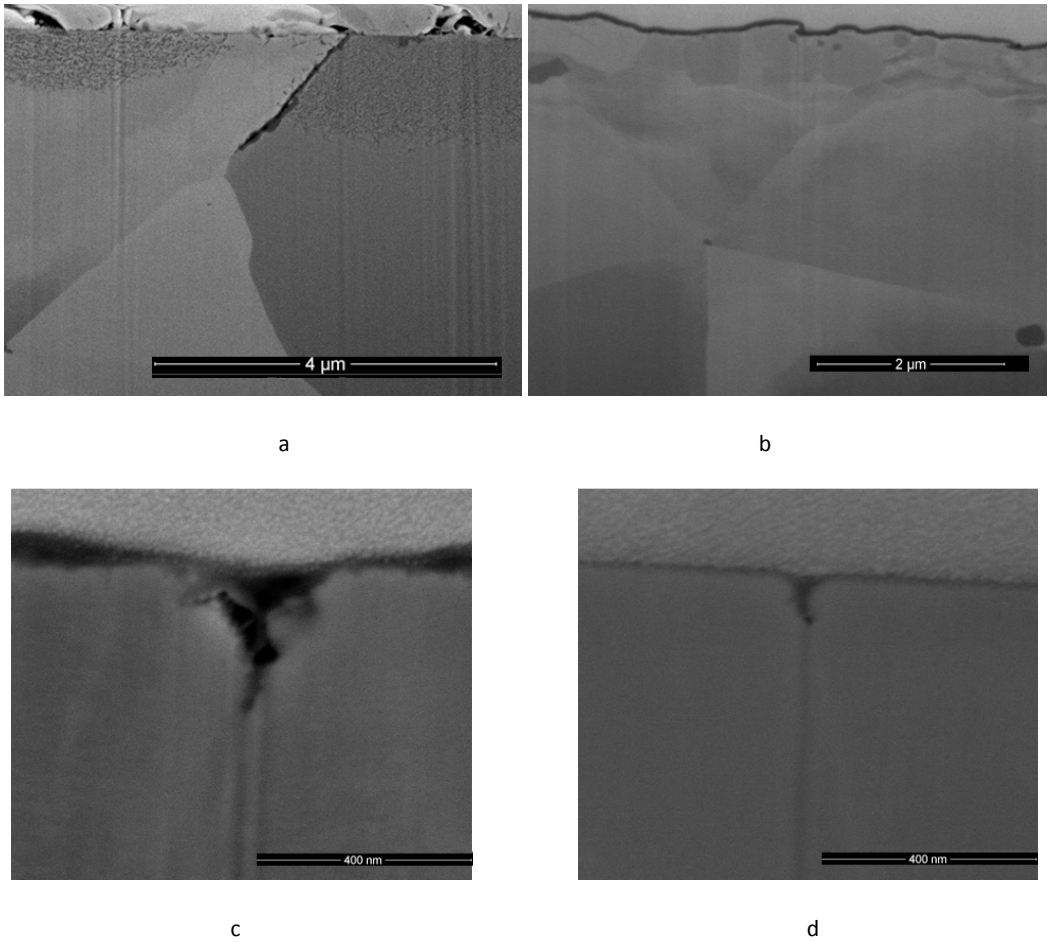

Figure 8 . FIB SE images showing cross-sections from 500°C testing after 500 h of exposure. (a) SE image of the OPS surface shows deep internal oxidation in adddtion to preverential oxidation of the grain boundaries. (b) SE image of the P600 surface (b) shows a contiuous oxide forming in preference to the internal oxide on the OPS surface. c and d are cross-sections from 500 h tests at 400°C and 350°C respectivly. All tests are from a ratio of 20.

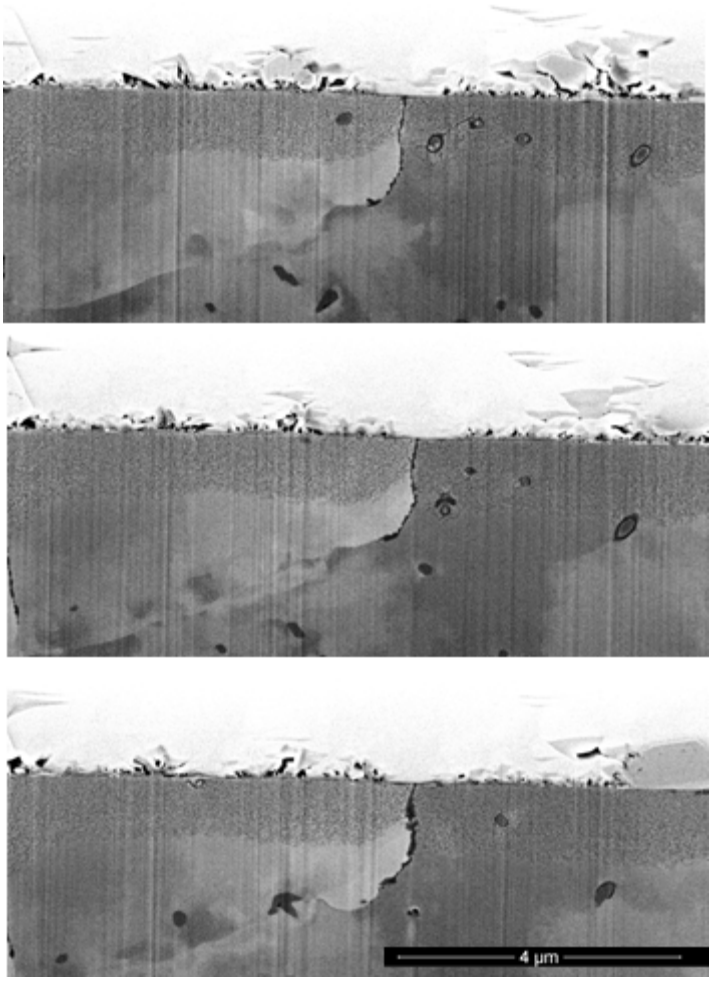

Figure 9. FIB SE images of cross-sections obtained by serial sectioning a 500°C hydrogenated steam sample. The oxidised feature on the right believed to be carbide is seen to draw the oxide beyond the internally oxidised zone.

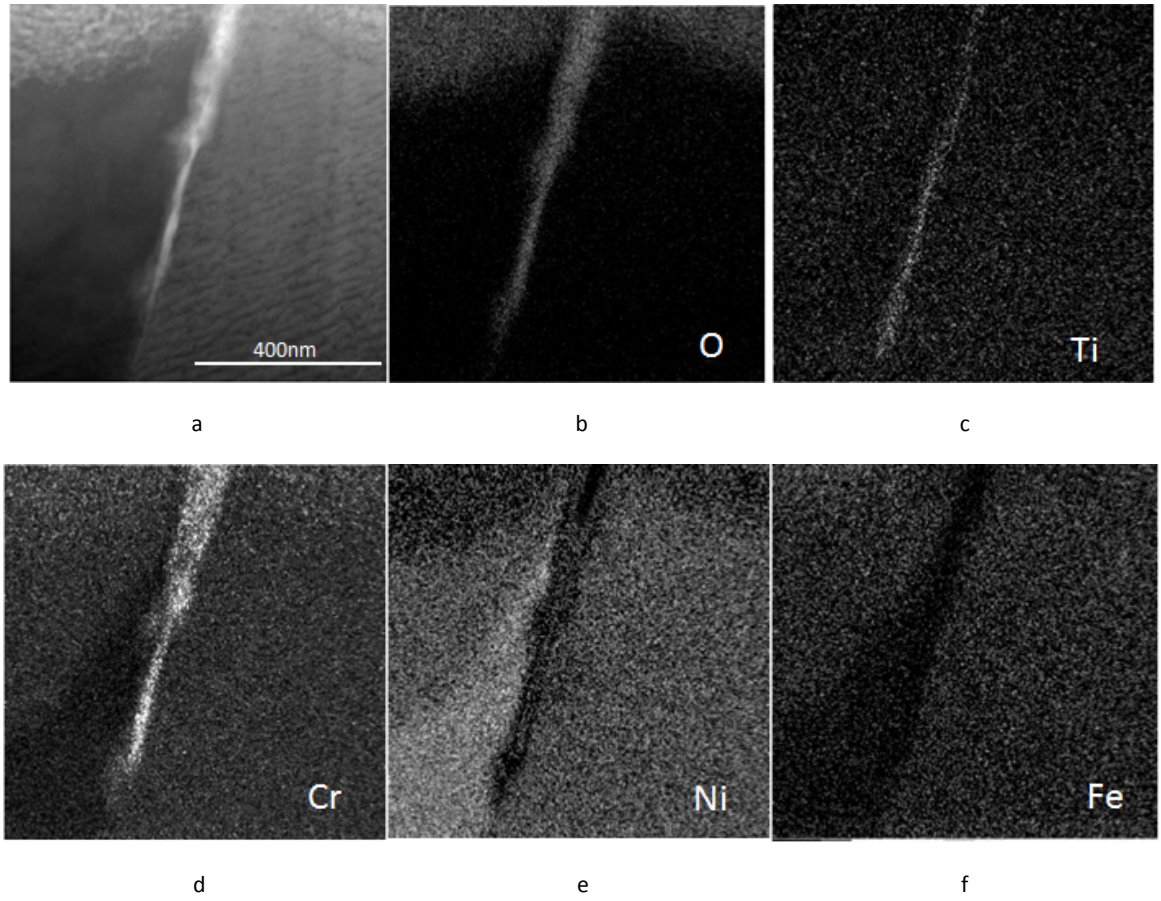

Figure 10 (a) bright-field STEM image and (b)-(f) corresponding SDD EDX spectrum images of an intergranular oxide penetration in the AR forging oxidised in hydrogenated steam at 500°C. Note the presence of Ti enrichment in the penetration. Also, note the Ni enrichment in the left-hand grain and the associated Cr and Fe depletion.

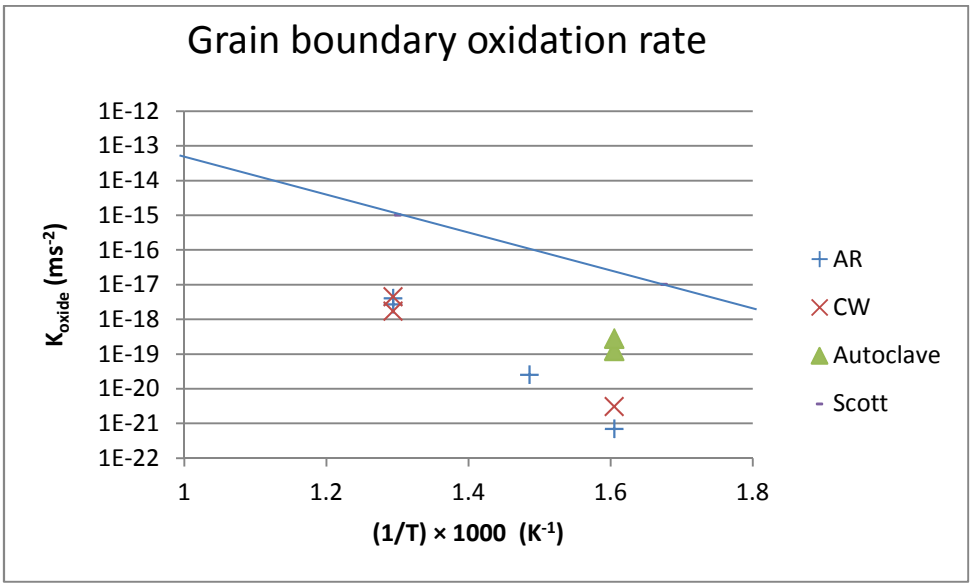

Figure 11 Measured oxidation rates in steam are consistent with the diffusion data obtained by Goto et al [5] and is significantly less then calculated by Scott. However a large variation is seen as a result of the oxidising systems pressure